Appl. Phys. B 68, 741–747 (1999) / DOI 10.1007/s003409901445

Applied Physics B
Lasers
and Optics

Analysis of degenerate four-wave mixing spectra of NO in a $CH_4/N_2/O_2$ flame

R.L. Farrow*, D.J. Rakestraw

Combustion Research Facility, P.O. Box 969, M.S. 9055, Sandia National Laboratories, Livermore, CA 94550, USA
(Fax: +1-925/294-2276, E-mail: farrow@ca.sandia.gov)

Received: 15 September 1998/Revised version: 18 November 1998/Published online: 24 February 1999

Abstract. We report comparisons of degenerate four-wave mixing (DFWM) spectra of NO measured in a $CH_4/N_2/O_2$ flame to spectral simulations based on a two-level theory for stationary, saturable absorbers by Abrams et al. Temperatures determined from least-squares fits of simulations to experimental spectra in the $A^2\Sigma^+ \leftarrow X^2\Pi^+(0,0)$ band are compared to temperatures obtained from OH absorption spectroscopy and a radiation-corrected thermocouple. We find that DFWM rotational temperatures derived from Q-branch spectra agree with thermocouple and are independent of pump laser intensity for low to moderate saturation ($I \approx I_{sat}$). However, the temperatures are systematically low and depend on pump intensity if the analysis neglects saturation effects. We demonstrate a method for obtaining an effective pump saturation intensity for use with the two-level model. This approach for analyzing saturated DFWM line intensities differs from previous work in that the use of the theory of Abrams et al. rather than a transition-dipole-moment power law allows treatment of a much wider range of saturation. Based on the observed signal-to-noise ratio an NO detection sensitivity of 25 ppm is projected, limited by a DFWM background interference specific to hydrocarbon flames.

PACS: 33; 42.65

Degenerate four-wave mixing (DFWM) is a nonlinear optical process that has been widely applied for optical phase conjugation [1], Doppler-free spectroscopy, and time-resolved spectroscopy [2]. More recently, resonant DFWM has been investigated as a noninvasive probe of trace species in combustion [3–5]. As the DFWM signal is generated in a coherent beam, the technique is especially well-suited for measurements in relatively inaccessible or luminous environments. Essentially an absorption-based technique, DFWM complements emission techniques such as laser-induced fluorescence (LIF), allowing the detection of a wider range of species.

Early demonstrations of the potential of DFWM as a combustion diagnostic involved the detection of Na atoms seeded in flames by Pender and Hesselink [6] and the detection of flame-generated OH by Ewart and O'Leary [7]. Flame temperature measurements by DFWM were obtained by Dreier and Rakestraw [8], who analyzed rotational intensities of saturated DFWM spectra of OH assuming a square-law dependence on the Einstein B coefficient. By measuring the distribution of rotational line intensities of NO as a function of laser intensity, Farrow et al. [9] showed that the square-law dependence is valid in the moderately saturated regime, but that a significantly higher-order dependence (up to quartic) is observed for lower laser intensities. The best-fit power law was shown to depend on the degree of saturation, implying that a simple power law would yield laser-power-dependent temperatures. Thus, temperatures are typically analyzed using a power law appropriate for the saturation regime; e.g., linear in B coefficient for strong saturation [10], quadratic for moderate saturation [11, 12], and quartic for low saturation [13]. Klamminger et al. [14] developed a technique for determining the best-fit power law of the transition dipole moment (which is proportional to $B^{1/2}$) for any given saturation regime, and used the law to measure temperatures of NaH molecules by DFWM. Flieser et al. [15] applied this method in measuring temperatures in an oxyacetylene flame using DFWM of NO.

In this paper we report comparisons of DFWM spectra of NO measured in a $CH_4/N_2/O_2$ flame to spectral simulations based on a two-level theory for stationary, saturable-absorbers by Abrams et al. [16]. Temperatures determined from least-squares fits of simulations to experimental Q_1/Q_{21} spectra in the $A^2\Sigma^+ \leftarrow X^2\Pi^+(0,0)$ band are compared to temperatures from OH absorption spectroscopy and radiation-corrected thermocouples. Attention is given to the effects of saturation on the DFWM temperatures. We demonstrate a method for obtaining an effective saturation intensity (I_{sat}) for use in the simulation. This approach for

* Corresponding author

analyzing saturated DFWM line intensities differs from previous work in that the use of the saturation theory of Abrams et al. rather than a dipole power law allows treatment of a much wider range of saturation. We also report NO detection sensitivity and interferences specific to hydrocarbon flames. This work extends a previous DFWM study of NO in clean H_2/O_2 flames [17] that used the moving-absorber theory of Abrams et al. [16] and did not treat saturation or determine temperatures.

1 Experiment

DFWM measurements were performed using a near-phase-conjugate geometry similar to that of [17]. Three UV beams derived from a pulsed dye laser were directed into the post-flame gases of a $CH_4/N_2/O_2$ flat flame. In this geometry the forward and backward pump beams are not precisely counter-propagating, but the backward beam intersects the other beams at a slight downward angle ($\approx 1°$). The signal beam then forms a similar downward angle with respect to the probe beam, allowing the former to be collected with a "scraper" mirror rather than sampled with a beam-splitter [17]. This geometry increased the signal collection efficiency and decreased stray light. The beam radii were ≈ 0.1 cm and the angle between the forward pump and probe beams was 4°, resulting in an interaction length of < 2.0 cm. The beams were vertically polarized and no analyzer polarizer was used in the detection system. The probe-beam intensity was 25% of the pump beams, which were of roughly equal intensity. To reduce stray light we focused the signal beam through a 25-μm pinhole. In addition, a 23-nm bandpass interference filter centered at 220.3 nm was placed in front of the DFWM detector, a side-on photomultiplier tube (Hamamatsu R955). To maximize the number of photoelectrons per photocurrent pulse without incurring nonlinearities, we wired the photomultiplier tube socket to use only five of the nine available dynodes. The output current was integrated using a sensitive charge preamplifier (EG&G Ortec 142B; 0.5 V/pC), digitized, and recorded by a computer. A correction for the wavelength-dependent response of the signal collection mirrors and detector was performed. We measured the response by tuning the laser over the region of interest, measuring the attenuated beam intensity, and comparing the response of the signal collection system to that of a spectrally flat pyroelectric detector.

We used a grating-tuned dye laser (Lambda-Physik 2002) as the excitation source, pumped by a frequency-doubled, injection-seeded Nd:YAG laser. The fundamental dye output was frequency doubled and sum-frequency mixed with the Nd:YAG laser fundamental to obtain ≈ 1 mJ/pulse near 226 nm, with a full-width at half maximum (FWHM) linewidth of 0.17 cm^{-1}. For most spectral measurements the laser frequency was stepped by 0.05 cm^{-1} and measurements from 12 laser shots were averaged. Line shape measurements were performed using an intra-cavity etalon that narrowed the laser bandwidth to 0.04 cm^{-1} in the visible, or an estimated 0.06 cm^{-1} in the UV. The pulse-averaged laser intensity was stabilized using a photoelastic modulator (Hinds International PEM-80) and polarizer. To account for pulse-to-pulse fluctuations in the signal measurements (up to ±50%) we normalized for laser energy fluctuations using the method described in [17]. This normalization divides the raw signal by a function involving the laser pulse energy and an effective I_{sat}, based on the saturation expression of the two-level theory of Abrams et al. [16]. The method is an approximation since the I_{sat} varies by transition, but it provides a better normalization than assuming an I^3 dependence.

Simultaneously with the DFWM measurements, we measured beam absorption by using pyroelectric detectors (Molectron J3-05) to measure the ratio of the transmitted to incident probe beam energy. The peak absorption by a strong NO Q-branch line was less than 5% over the estimated 4-cm beam path. No correction to the DFWM signal for absorption was attempted.

The Hencken-type burner used in these studies was constructed of a rectangular steel honeycomb encompassing a 2.2×4.7 cm^2 array of small stainless-steel tubes connected to the CH_4 supply. A mixture of N_2 and O_2 flowed from the honeycomb, mixed with the CH_4 flow and burned essentially as a lean premixed flame < 1 mm above the burner surface. The CH_4, N_2, and O_2 flow rates were 2.16, 14.9, and 6.5 standard l/min (slpm), respectively, corresponding to an equivalence ratio of 0.66. A shield flow of 5.1 slpm of N_2 emerged from the honeycomb surrounding the fuel-tube array. The pump beams were centered over the burner, parallel to the longer dimension and 0.75 cm above the surface.

Using a 4-μm diameter, Pt/Pt-13%Rh thermocouple corrected for radiation and conduction losses, we obtained a temperature of 2040 ± 120 K at the center of the beam-crossing location. However, in the outer boundaries of the flame the measured temperature was 2240 ± 160 K (uncertainties estimated at 3/4 of the radiation corrections). This temperature gradient apparently resulted from a reduced output of the fuel tubes near the burner center, some of which were fused closed. A calculation using STANJAN [18] assuming thermodynamic equilibrium, neglecting all heat losses and based on the total reactant flow rates predicted a temperature of 2202 K. This result is consistent with the thermocouple temperature at the flame boundary. Assuming the stoichiometry was 10% leaner in the flame center due to the damaged fuel tubes, an equilibrium temperature of 2070 K is calculated, reasonably consistent with the thermocouple value at the center.

A second estimate of the center flame temperature was obtained by fitting OH absorption spectra of the R_1 branch in the $A^2\Sigma^+(v'=0) \leftarrow X^2\Pi(v''=1)$ transition at 281 nm. We measured the transmittance of a 2-mm diameter collimated beam directed along the same path as the DFWM pump beams. Low pulse energies (< 2 μJ) were used to avoid saturation. We fitted the resulting absorption spectrum assuming

$$I(\nu) = I_0 \exp\left[-\sum_{J''} S_{J''} P_{J''} g\,(\nu - \nu_{J''}) \right] ,$$

where $g\,(\nu - \nu_{J''})$ is the normalized line shape function for the transition from ground rotational level J'' (taken as a Voigt profile with the homogeneous linewidth varied for best fit), $S_{J''}$ is the rotational line strength, and $P_{J''}$ is a population factor equal to $\exp(-E_{J''}/kT)$. Using line strengths given by Chidsey and Crosley [19], we varied the $P_{J''}$ factors for best fit and obtained a rotational temperature of 2225 K. This path-averaged result is expected to be biased toward the

higher temperatures at the flame boundary because of the increased concentration of OH in that region.

2 Simulation of DFWM spectra

Theoretical descriptions of molecular, as opposed to atomic, DFWM spectra are complicated by closely spaced resonances, rotational level degeneracies, and collisional effects involving changes in molecular angular momentum. While some of these effects have been considered in perturbative theories [20] and non-perturbative calculations [21], a comprehensive theory is not available nor likely to be practical for data analysis. However, the consideration of simplified two-level systems has resulted in tractable signal-intensity expressions useful in diagnostic applications. For cases where saturation can be neglected, Abrams et al. [16] derived expressions for two-level moving absorbers with Doppler- and homogeneously broadened resonances probed in a collinear, phase-conjugate geometry. Here, the signal intensity varies as μ^8, where μ is the transition dipole moment of the nondegenerate transition. Theoretical spectra based on this theory have been compared to DFWM spectra of NO measured in an H_2/O_2 flame [17]. These calculations used effective values of μ (averaged over m levels) obtained from one-photon rotational line strengths. Relative line intensities of the theoretical and experimental spectra were in good agreement, though a quantitative comparison was not attempted.

For practical measurements of trace species by DFWM, significant saturation will typically be present. Indeed, signal strength, reproducibility, and sensitivity to collisional environment are normally optimized [22] by operating near $I/I_{\text{sat}} \approx 1$. Here the two-level, stationary-absorber theory of Abrams et al. [16], which treats saturating pump beams, is attractive. This theory has been shown to provide a good description of the saturation behavior of DFWM lines in the A-X (0,0) O_{12}-branch of NO [9], and has been used to simulate complex, overlapping DFWM spectra of C_2 in the unsaturated regime [13]. The omission of Doppler broadening of the absorption lines results in theoretical line shapes that are too narrow; nevertheless, we expect relative intensities of isolated lines, from which temperature is derived, to be reasonably well described [9]. We used the following expressions to calculate the phase-conjugate intensity:

$$I_{\text{c}}(\omega) \propto I_{\text{probe}} \left| \sum_{J''J'} \beta_{J''J'}(\omega) \right|^2 , \tag{1}$$

$$\beta_{J''J'}(\omega) = \frac{\omega_{J''J'} \Delta n_{J''J'} \mu^2_{J''J'}}{\gamma_{J''J'}} \frac{i + \delta_{J''J'}}{1 + \delta^2_{J''J'}} \frac{2I/I_{\text{sat}}^{J''J'}}{\left(1 + 4I/I_{\text{sat}}^{J''J'}\right)^{3/2}} . \tag{2}$$

Equations (1) and (2) are based on the results of Abrams et al. [16] assuming pump beams of equal intensity I and negligible absorption. Here,

$$\delta_{J''J'} = \frac{\omega - \omega_{J''J'}}{\gamma_{J''J'}} \tag{3}$$

is the normalized detuning from each transition, $\mu_{J''J'}$ is the transition dipole moment, and

$$I_{\text{sat}}^{J''J'} = \frac{\varepsilon_0 c \hbar^2 \gamma_{J''J'} \Gamma_{J''J'}}{2\mu^2_{J''J'}} \left(1 + \delta^2_{J''J'}\right) \tag{4}$$

is the transition-dependent saturation parameter. Also, $\gamma_{J''J'}$ is the coherence dephasing rate, $\Gamma_{J''J'}$ is the population decay rate, and $\Delta n_{J''J'}$ is the unperturbed population difference between the upper and lower level of a transition (for NO $A \leftarrow X$ transitions the upper-level population can be neglected at 2000 K). Note that overlapping lines, including the nearly degenerate Q_1 and Q_{21} transitions, are treated by adding amplitudes before squaring (1). We chose to investigate the overlapping Q-branch lines rather than the P_1 or R_2 branches due to the significantly larger B coefficients of the Q branch.

Expressions (1)–(4) are valid for a weak probe-beam intensity and an arbitrarily high pump-beam intensity. Nevertheless, several simplifying assumptions were made in applying the theory to NO in flames. In addition to neglecting grating washout from thermal motion (mainly affecting overall signal strength) and Doppler broadening of the absorption line shapes (mainly affecting DFWM line shapes), we assumed that each transition had the same collisional width. This assumption is supported by the fact that collision widths of NO measured at room temperature [23] exhibit no measurable dependence on J'', and we observed none in moderate-resolution flame spectra described below. We also neglected cross-over resonances [24] associated with the nearly degenerate Q_1 and Q_{21} transitions. To our knowledge, these contributions have only been treated for the case of low saturation; hence, the results [24] cannot be applied here. The cross-over contributions are expected to be most important for low-J transitions; because we measured mainly high-J lines they should have little effect on the derived temperature. (We estimated the cross-over contribution to the intensity of $Q_1/Q_{21}(6.5)$ to be less than 1% in the low-saturation limit, and decreasing with higher J.) In applying a two-level model, rotational level degeneracy is neglected insofar as four-wave mixing processes involving more than two levels at a time are not included. Perturbative treatments of degenerate rotational levels are given in [20] and [24], where it is shown that m-level degeneracies require a coherent summation, over all initial and final m states, of four-photon transition amplitudes (i.e., summed products of four dipole-moment matrix elements). The resulting four-photon line amplitudes can differ from amplitudes used in the present model, which are proportional to one-photon transition moments raised to the fourth power. Level degeneracies are approximated by using in (2) and (4) an m-averaged transition moment obtained from the Einstein absorption coefficient:

$$\mu^2_{J''J'} = \frac{\varepsilon_0 \hbar^2}{\pi} B_{J''J'} . \tag{5}$$

This relation yields correct expressions for the absorption coefficient when used in the model of Abrams et al. [16], but differs by a factor of three from the expression given by Hilborn [25]. The NO B coefficients were computed using expressions given by Paul [26].

To compare the theoretical predictions of relative line intensities with experiment, we performed nonlinear least-

squares fits of (1) to measured DFWM spectra. The effects of laser bandwidth were approximated by convolving the theoretical spectra with a Gaussian profile (the laser linewidth, 0.17 cm^{-1} FWHM, was comparable to that of the transitions). Line positions were varied slightly for best fit to account for scan nonlinearities. The DFWM fitting program used the minimization routine STEPIT [27] and is designed to efficiently analyze spectra with non-continuous frequency scans. Best-fit temperatures from DFWM spectra were compared to results from thermocouple and OH absorption measurements.

3 Results and discussion

The upper panel of Fig. 1 shows an experimental DFWM spectrum of the NO Q_1- and Q_{21}-branch region obtained in the flame. All of the transitions, with the exception of those marked with asterisks, are assigned to branches of NO and are so labeled. Note that the small splittings between main and satellite lines are not resolved owing to collision broadening and the laser linewidth. The additional features have been assigned to Schumann–Runge transitions of O_2. Owing to the presence of a weak DFWM background signal, the NO signal-to-noise ratio (SNR) was found to be 600 : 1, about a factor of three lower than that observed in an H_2/O_2 flame [17], where a similar background was not observed. Interestingly, the optimum SNR occurred for modest pump intensities of $2–4 \times 10^5$ W/cm^2, well below the average I_{sat} (see below). At higher intensities the NO signal increased sublinearly due to saturation while the background signal continued to increase with a roughly cubic intensity dependence. To estimate the detection sensitivity for NO we determined the path-averaged NO concentration from probe-beam absorption measurements. By comparing the line-integrated absorbance of the $Q_1(16)$ transition observed in the flame to that in a room-temperature cell of 100 mTorr of NO in 340 Torr of N_2 (conditions giving a similar linewidth), we obtained a path-averaged NO concentration of 620 ppm in the flame, assuming an average temperature of 2130 K. This result agrees well with the value of 603 ppm determined by measuring the increase in flame absorption from standard additions of NO to the input gases. Based on our signal-to-noise ratio we calculate a detectivity of ≈ 25 ppm of NO based on a SNR of 1 and a 2-s integration time.

To determine effective saturation parameters for the data of Fig. 1 we measured the signal from a selected line as

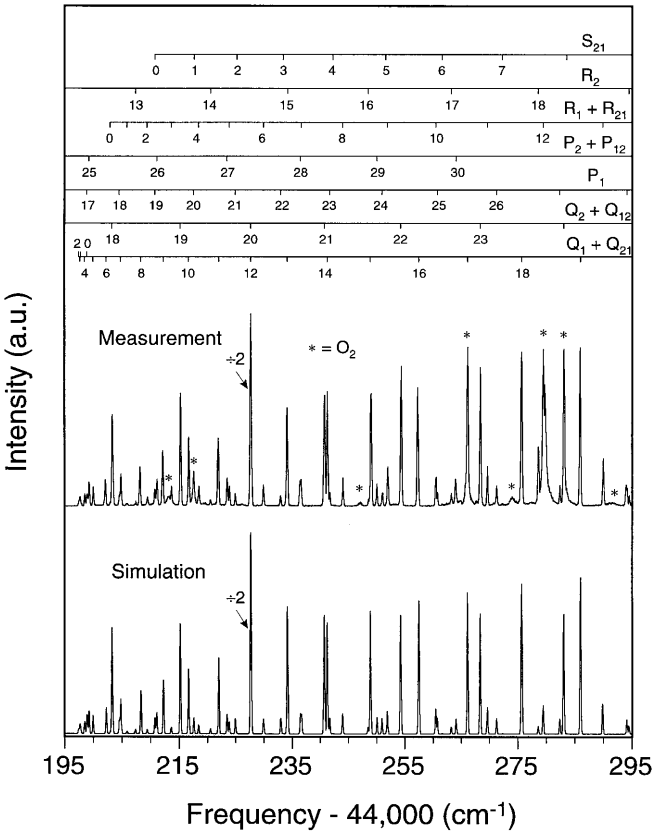

Fig. 1. Measured and simulated DFWM spectra of NO and O_2 in a $CH_4/N_2/O_2$ flame. The NO lines belong to the $A^2\Sigma^+ \leftarrow X^2\Pi^+(0,0)$ system. O_2 transitions are marked by *asterisks* and are not included in the simulation. The simulation is based on a theory for DFWM in a system of two-level, non-degenerate, stationary absorbers by Abrams et al. [16] and includes modest saturation by the pump beams. The nearly degenerate main and satellite transitions are treated as degenerate in the branch identifiers; the labels indicate $J'' - 1/2$. The prominent line near 44 223 cm^{-1} has been reduced in vertical scale by a factor of 2

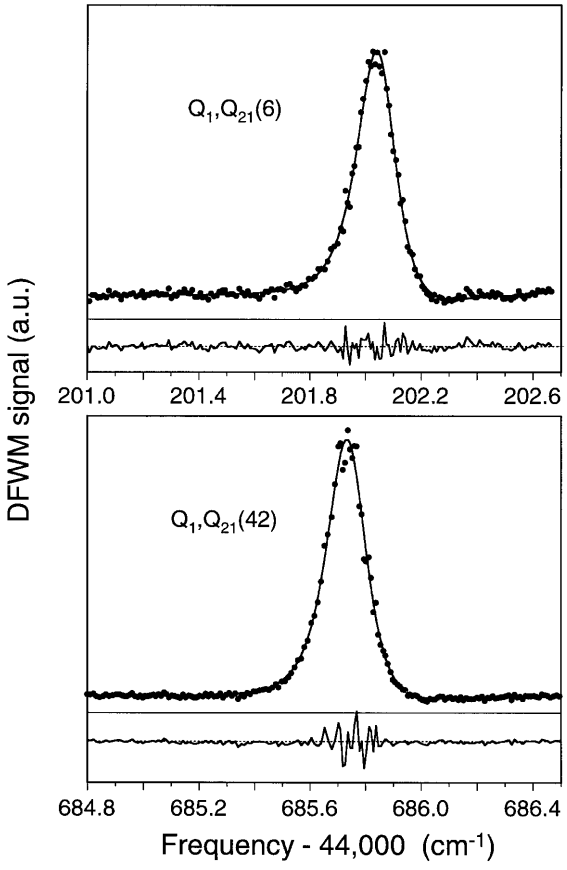

Fig. 2. Measured and best-fit simulated DFWM spectra of two transitions in the $A^2\Sigma^+ \leftarrow X^2\Pi^+(0,0)$ system of NO, plotted by *filled circles* and a *smooth line*, respectively. The difference between data and fit is also indicated. The simulation is based on a theory for DFWM in a system of two-level, non-degenerate, moving absorbers by Abrams et al. [16] and does not include saturation effects. The laser linewidth was 0.06 cm^{-1} (FWHM). A weak DFWM background heterodynes with the resonances, resulting in slight asymmetries and dips on the high-frequency sides of the peaks. Both best-fit homogeneous linewidths were 0.18 ± 0.02 cm^{-1}; all investigated lines between $N'' = 6$ and 42 were consistent with this linewidth

a function of pump intensity, up to the maximum available laser energy where $I \approx I_{sat}$. We fitted the resulting saturation curve with the expression $(I/I_{sat})^2 \,/\, (1+4I/I_{sat})^3$ from (1) and (2), varying the saturation intensity I_{sat} for best fit. Values of I_{sat} for other transitions were scaled from this result using (4) and (5) and the line-dependent B coefficients [26]. (Recall $\gamma_{J''J'}$ and $\Gamma_{J''J'}$ are taken to be constant for all lines.) For the nearly degenerate $Q_1(11)$ and $Q_{21}(11)$ transition we obtained a best-fit value of $I/I_{sat} = 0.08 \pm 0.03$ (for the value of I used in Fig. 1). We note that the $Q_1(11)$ contribution to the fitted curve is dominant [> 4 times that of $Q_{21}(11)$]. Determining I from the measured pump-pulse energy, pulse width, and beam diameter gave $I_{sat} \approx 7\,\mathrm{MW/cm^2}$, with an uncertainty factor of $2-3$ arising mainly from the measurement of I. The result is nevertheless significantly lower than the value of $60\,\mathrm{MW/cm^2}$ calculated for $Q_1(11)$ from (4). The calculation assumed $\gamma_{J''J'} = \Gamma_{J''J'}$ but the population relaxation rate is probably lower than the coherence dephasing rate due to pure dephasing contributions, decreasing the calculated value of I_{sat}. In addition, adding the "missing" factor of 3 in (5) would also decrease I_{sat}.

Homogeneous linewidths of the transitions were investigated by acquiring higher resolution DFWM spectra of various Q_1/Q_{21} lines. We inserted an angle-tunable intracavity etalon in the dye laser and obtained a UV linewidth of $0.06 \pm 0.02\,\mathrm{cm^{-1}}$. Figure 2 shows two typical scans for $N'' = 6$ and 42, measured with $I/I_{sat} < 0.05$ and plotted using filled circles. The solid lines show the results of least squares fits of line shape simulations based the moving absorber theory of Abram et al. [16] (which includes Doppler effects but neglects saturation). Varied for best fit were a vertical offset accounting for stray light, a weak nonresonant DFWM contribution discussed below, and the homogeneous linewidth. We obtained $0.18 \pm 0.02\,\mathrm{cm^{-1}}$ (FWHM) for the latter, which did not vary with N'' within experimental uncertainty.

The weak nonresonant signal originated from a four-wave mixing process as it required the presence of all three input beams. We included it in the simulation as a purely real, positive background consistent with the heterodyning observed in the NO resonance (note the slight dip in the higher-frequency wing and the slight asymmetry in Fig. 2). We expect the background is associated with a weak broadband absorption (2%–3%) observed in the present CH_4 flame. We observed a similar broadband absorption and accompanying DFWM background in other hydrocarbon flames using laser wavelengths of 250 nm and below [28, 29]. Although we did not investigate the use of crossed polarizations here, in other DFWM studies [29] of OH and O_2 at 248 nm we found that the background could be canceled using a cross-polarized forward pump beam, but at a cost in resonant signal strength. This observation, together with a two-color FWM investigation in [28], indicate that the background is likely due to DFWM by thermal gratings. Such gratings are generated from heat released by collisional quenching of the broadband absorbers [5]. The thermal-grating mechanism differs from the population-grating mechanism treated by (1)–(5), and can exhibit higher saturation intensities. Danehy et al. [30] have shown that DFWM of NO in high-temperature regions of CH_4/air flames is dominated by scattering from population gratings.

A simulation of the Q_1/Q_{21}-branch spectral region is shown in the lower panel of Fig. 1. The simulation was performed using the stationary absorber model as implemented in (1)–(5), and assuming $I/I_{sat} = 0.08$ as measured for $Q_1(11)$. The values of I/I_{sat} for other transitions were scaled from this result as described previously. The collisional relaxation rates $\gamma_{J''J'}$ and $\Gamma_{J''J'}$ were assumed equal to $0.18 \pm 0.02\,\mathrm{cm^{-1}}$ (FWHM) for all transitions. Peak intensities in the simulation are seen to be in qualitative agreement with the NO Q_1 and Q_2 lines dominating the experimental spectrum, except where accidental overlaps with O_2 lines occur (the latter are marked with asterisks and were not included in the simulation). While relative peak intensities are well described, the calculated

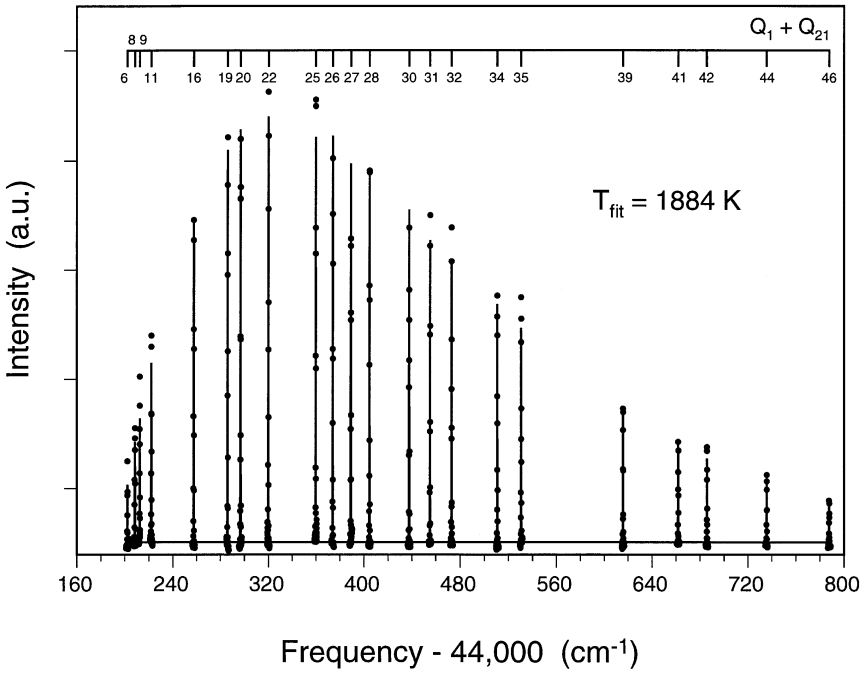

Fig. 3. Measured and best-fit simulated DFWM spectra of selected Q_1/Q_{21} transitions in the $A^2\Sigma^+ \leftarrow X^2\Pi^+(0,0)$ system of NO, plotted by *filled circles* and a *smooth line*, respectively. The simulation is based on a theory for DFWM in a system of two-level, non-degenerate, stationary absorbers by Abrams et al. [16] and omits modest saturation by the pump beams. The spectra resemble "stick" plots because of the narrow linewidths, $< 0.2\,\mathrm{cm^{-1}}$ FWHM, compared to the tuning range

line shapes are narrower than experiment as a result of neglecting Doppler effects. The most significant disagreements involve the total intensities of branches; e.g., the P_1-branch lines tend to be overpredicted relative to the Q_1 branch. We attribute this effect to the approximate treatment of rotational level degeneracies; i.e., using one-photon rather than the four-photon line amplitudes discussed previously. Comparing DFWM intensities predicted by the present method to the those of the latter [20, 24], we found that overall branch intensities differ by up to 50% but that the relative line intensities within individual branches agree closely for $N'' > 5$.

To quantitatively test the prediction of relative line intensities by the DFWM model, we compared temperatures obtained from least-squares fits of DFWM spectra to the thermocouple measurement at the beam-crossing location. Twenty-four pairs of transitions in the Q_1/Q_{21} branch were selected based on freedom from overlap with other lines, and data were acquired during short (2-cm^{-1}) frequency scans through each line pair. The short scans were obtained in sequence, with the dye laser being scanned rapidly between the selected lines. Figure 3 shows a comparison of an experimental spectrum (data points) with a simulation (solid line) *assuming no saturation* and varying the temperature for best fit. (The spectra resemble "stick" plots because of the narrow linewidths, $< 0.2\,\mathrm{cm}^{-1}$ FWHM, compared to the large scan width.) The best-fit temperature, 1884 K, is signicantly lower than the thermocouple measurement of 2030 K. A systematic underprediction of the low rotational lines is observed, despite adjusting the temperature for best fit.

As we increased the incident laser intensity (using neutral density filters to maintain roughly the same maximum signal intensity) we observed a systematic decrease in the best-fit temperature when saturation was neglected. Plotted with filled triangles in Fig. 4 are fitted temperatures for various laser intensities, plotted in units of I/I_{sat} for $Q_1(11)$. For

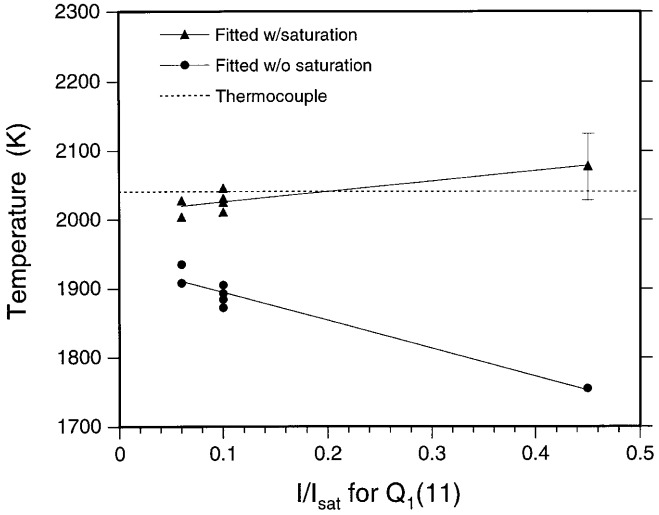

Fig. 4. Temperatures from fits of Q_1/Q_{21} transitions in DFWM spectra and from a radiation-corrected thermocouple. If saturation is neglected in analyzing DFWM spectra, the resulting temperatures are anomolously low and dependent on laser intensity (*filled circles*). If pump saturation is included the temperatures are in good agreement with the thermocouple and are independent of laser intensity

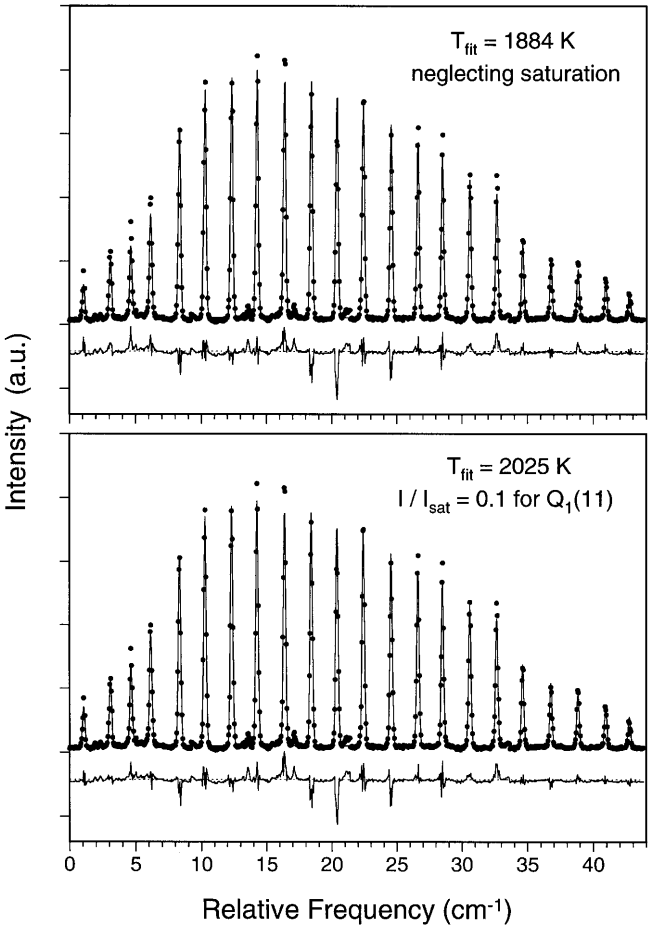

Fig. 5. Comparison of measured and best-fit simulated DFWM spectra of selected Q_1/Q_{21} transitions of NO, plotted by *filled circles* and a *smooth line*, respectively. The transitions are the same as those shown in Fig. 3 but plotted with frequency gaps removed to allow closer examination of the fits. The *upper panel* shows the same fit as Fig. 3, which neglects saturation. The *lower panel* shows a fit including pump saturation

comparison, the horizontal dashed line indicates the thermocouple measurement. The best-fit temperature from DFWM is seen to decrease with increasing laser intensity, dropping by 150 K at the highest intensity. This effect results from line-dependent values of I/I_{sat}: as the laser intensity increases, lines with larger B coefficients are more saturated and consequently exhibit relatively lower signal strength. As the higher N lines of OH Q branches have larger B coefficients, the result is a lower apparent temperature.

For moderate saturation intensities, we found that the observed variation in best-fit temperature with laser intensity could be corrected by accounting for saturation. As input to the model we used the measured saturation parameter for $Q_1(11)$ and calculated I/I_{sat} for other lines as before. The result was a slightly improved fit and significantly higher best-fit temperatures. A comparison between such fits with saturation neglected and included is shown in Fig. 5, plotted with frequency gaps removed to better reveal the fits. The quality of the fit with saturation is only slightly improved near the bandhead and at high rotational lines, though the best-fit temperature is substantially higher. Temperatures obtained in this manner were constant within experimental uncertainty for saturation parameters of 0.06 to 0.45. In addition, the tem-

peratures were in excellent agreement with the thermocouple result as shown by the filled circles in Fig. 4. However, the saturation-corrected DFWM temperatures are confirmed only to within the thermocouple uncertainty of ± 120 K; a more detailed examination awaits comparisons to coherent anti-Stokes Raman spectroscopy measurements in an isothermal flame or furnace.

4 Summary and conclusions

Spectral simulations using a stationary, saturable absorber model were in good agreement with experimental DFWM peak intensities as long as saturation was considered. Temperatures derived from fitting selected Q_1/Q_{21}-branch lines were in good agreement with thermocouple estimates, even for pump intensities approaching I_{sat}. We demonstrated the feasability of obtaining effective I_{sat} parameters used in the theory directly from measurements of signal versus laser intensity. These results justify the use of the two-level stationary absorber theory of Abrams et al. for extracting rotational temperatures. However, the following caveats are noted: (1) moderate saturation ($I < I_{\text{sat}}$), (2) parallel laser polarizations, and (3) analysis of one branch at a time (since relative intensities between branches are not quantitatively predicted). Caveats (2) and (3) could be addressed by developing a theory that treats the effects of degenerate rotational levels together with saturation. Williams et al. [31] and Lehr et al. [32] demonstrated that geometrical factors derived from perturbative treatments [20] of DFWM, when used with a power-law treatment of saturation, successfully describe relative saturated line intensities for various polarization geometries. It remains to be seen whether a more rigorous treatment of saturation such as that by Abrams et al. can be combined with the use of geometrical factors.

Our results show that DFWM is useful for characterizing NO in methane/air flames at concentrations of a few hundred ppm. We obtained an estimated detectivity limit of 25 ppm for time-averaged measurements, limited by a background DFWM signal not previously observed in H_2/air flames. While spatial resolution was poor along the beams (≈ 2 cm), sub-mm resolution is possible in a perpendicular direction. Although LIF offers greater sensitivity and spatial resolution for NO detection, the reduced sensitivity of DFWM to collisional quenching and its collimated signal are advantageous for some applications.

The use of pump intensities approaching I_{sat} generally results in improved SNR and decreased sensitivity to collisional broadening and quenching rates. However, in hydrocarbon-fueled flames at laser wavelengths of ≈ 250 nm and shorter, we observed a nonresonant DFWM background that limited sensitivity for weak resonant signals and precluded the use of strongly saturating laser intensities. The likely cause of this background is a thermal grating, which invites the use of shorter (subnanosecond) laser pulses to avoid probing the slowly forming thermal grating.

Acknowledgements. This work was supported by the United States Department of Energy, Office of Basic Energy Sciences, Division of Chemical Sciences.

References

1. R.A. Fisher (Ed.): *Optical Phase Conjugation* (Academic, New York 1983)
2. H.J. Eichler, P. Günter, D.W. Pohl: *Laser-Induced Dynamic Gratings* (Springer-Verlag, New York 1986)
3. R.L. Farrow, D.J. Rakestraw: Science **257**, 1894 (1992)
4. K. Kohse-Höinghaus: Prog. Energy Combust. Sci. **20**, 203 (1994)
5. A.C. Eckbreth: *Laser Diagnostics for Combustion Temperature and Species* (Gordon and Breach, Amsterdam 1996) pp. 479–511
6. J. Pender, L. Hesselink: Opt. Lett. **10**, 264 (1985)
7. P. Ewart, S.V. O'Leary: Opt. Lett. **11**, 279 (1986)
8. T. Dreier, D.J. Rakestraw: Opt. Lett. **15**, 72 (1990)
9. R.L. Farrow, D.J. Rakestraw, T. Dreier: J. Opt. Soc. Am. B **9**, 1770 (1992)
10. B. Yip, P.M. Danehy, R.K. Hanson: Opt. Lett. **17**, 751 (1992)
11. D.A. Feikema, E. Domingues, M.-J. Cottereau: Appl. Phys. B **55**, 424 (1992)
12. C.F. Kaminski, I.G. Hughes, G.M. Lloyd, P. Ewart: Appl. Phys. B **62**, 39 (1996)
13. C.F. Kaminsky, I.G. Hughes, P. Ewart: J. Chem. Phys. **106**, 5324 (1997)
14. A. Klamminger, M. Motzkus, S. Lochbrunner, G. Pichler, K.L. Kompa, P. Hering: Appl. Phys. B **61**, 311 (1995)
15. J. Flieser, K. Iskra, A. Morozov, G. Pichler, T. Neger: J. Phys. D: Appl. Phys. **31**, 402 (1998)
16. R.L. Abrams, J.F. Lam, R.C. Lind, D.G. Steel, P.F. Liao: "Phase conjugation and high-resolution spectroscopy by resonant degenerate four-wave mixing", in [1], pp. 211–284
17. R.L. Vander Wal, R.L. Farrow, D.J. Rakestraw: *High-resolution investigation of DFWM in the γ(0-0) band of nitric oxide*, in Twenty-Fourth Symposium (International) on Combustion (The Combustion Institute 1992) pp. 1653
18. STANJAN version 3.95, W.C. Reynolds, Stanford University
19. I.L. Chidsey, D.R. Crosley: J. Quant. Spectrosc. Radiat. Transfer **23**, 187 (1980)
20. S. Williams, R.N. Zare, L.A. Rahn: J. Chem. Phys. **101**, 1072 (1994)
21. T.A. Reichardt, R.P. Lucht: J. Opt. Soc. B **14**, 2449 (1997)
22. R.P. Lucht, R.L. Farrow, D.J. Rakestraw: J. Opt. Soc. Am. B **10**, 1508 (1993)
23. A.Y. Chang, M.D. Di Rosa, R.K. Hanson: J. Quant. Spectrosc. Radiat. Transfer **47**, 375 (1992)
24. E.J. Friedman-Hill, L.A. Rahn, R.L. Farrow: J. Chem. Phys. **100**, 4065 (1994)
25. R.C. Hilborn: Am. J. Phys. **50**, 982 (1982). The relation given by Hilborn includes an additional factor of 3 on the right-hand side. This discrepancy does not affect temperatures derived using (1)–(4), which depend only on relative line intensities, but does affect theoretical saturation intensities. The missing 3 may result from using a relation between the *B* coefficient and the absorption cross section that assumes a directed radiation field, while Hilborn's version of (5) is for an isotropic field
26. P. Paul: J. Quant. Spectrosc. Radiat. Transfer. **57**, 581 (1997)
27. STEPIT minimization software by J.P. Chandler: Quantum Chem. Program Exchange **11**, 307 (1976);
see http://www.osc.edu/cca/html_pages/qcpe, Sect. 1, QCPE 307
28. R.L. Farrow, M.N. Bui-Pham, V. Sick: *Degenerate Four-Wave Mixing Measurements of Methyl Radicals in Hydrocarbon Flames: Comparison with Model Predictions*, Twenty-Sixth Symposium on Combustion (International) (The Combustion Institute, Pittsburgh 1996) p. 975
29. To be published elsewhere
30. P.M. Danehy, P.H. Paul, R.L. Farrow: J. Opt. Soc. Am. B **12**, 1564 (1995)
31. S. Williams, R.N. Zare, L.A. Rahn: J. Chem. Phys. **101**, 1093 (1994)
32. L. Lehr, M. Motzkus, G. Pichler, K.L. Kompa, P. Hering: J. Chem. Phys. **104**, 9698 (1996)